Author/s:
Wojnilowicz, M;Laznickova, P;Ju, Y;Ang, CS;Tidu, F;Bendickova, K;Forte, G;Plebanski, M;Caruso, F;Cavalieri, F;Fric, J

Title:
Influence of protein corona on the interaction of glycogen–siRNA constructs with ex vivo human blood immune cells

Date:
2022-09-01

Citation:
Wojnilowicz, M., Laznickova, P., Ju, Y., Ang, C. S., Tidu, F., Bendickova, K., Forte, G., Plebanski, M., Caruso, F., Cavalieri, F. & Fric, J. (2022). Influence of protein corona on the interaction of glycogen–siRNA constructs with ex vivo human blood immune cells. Biomaterials Advances, 140, https://doi.org/10.1016/j.bioadv.2022.213083.

Persistent Link:
https://hdl.handle.net/11343/313843

Influence of protein corona on the interaction of glycogen–siRNA constructs with *ex vivo* human blood immune cells

Marcin Wojnilowicz[a,$,#], Petra Laznickova[b,c,#], Yi Ju[a,d], Ching-Seng Ang[e], Federico Tidu[b,f], Kamila Bendickova[b], Giancarlo Forte[b], Magdalena Plebanski[d], Frank Caruso*[a], Francesca Cavalieri*[g,h], Jan Fric*[b,i]

[a] Department of Chemical Engineering, The University of Melbourne, Parkville, Victoria 3010, Australia

[b] Center for Translational Medicine, International Clinical Research Center (ICRC), St Anne's University Hospital Brno, Pekarska 53, 656 91 Brno, Czech Republic

[c] Department of Biology, Faculty of Medicine, Masaryk University, Kamenice 5, 625 00 Brno-Bohunice, Czech Republic

[d] School of Health and Biomedical Sciences, RMIT University, Bundoora, Victoria 3083, Australia

[e] Bio21 Molecular Science and Biotechnology Institute, The University of Melbourne, Parkville, Victoria 3010, Australia

[f] Division of Cancer Biology, The Institute of Cancer Research: London, 123 Old Brompton Road, London SW73RP, Great Britain

[g] School of Science, RMIT University, Victoria 3000, Australia**.**

[h] Dipartimento di Scienze e Tecnologie Chimiche, Universita' degli Studi di Roma "Tor Vergata", Via della Ricerca Scientifica 1, 00133, Rome, Italy

[i] Institute of Hematology and Blood Transfusion, U Nemocnice 2094, 128 20 Prague 2, Czech Republic

[#] These authors contributed equally to this work

$ Current address: Commonwealth Scientific and Industrial Research Organisation (CSIRO) Manufacturing, Bayview Avenue, Clayton, Victoria 3168, Australia

Corresponding authors:

*E-mail: fcaruso@unimelb.edu.au

*E-mail: francesca.cavalieri@unimelb.edu.au

*E-mail: jan.fric@fnusa.cz

Abstract

Glycogen–nucleic acid constructs i.e., glycoplexes are emerging promising platforms for the alteration of gene expression and transcription. Understanding the interaction of glycoplexes with human blood components, such as serum proteins and peripheral blood mononuclear cells (PBMCs), is important to overcome immune cell activation and control biodistribution upon administration of the glycoplexes *in vivo*. Herein, we investigated the interactions of polyethylene glycol (PEG)ylated and non-PEGylated glycoplexes carrying siRNA molecules with PBMCs isolated from the blood of healthy donors. We found that both types of glycoplexes were non-toxic and were primarily phagocytosed by monocytes without triggering a pro-inflammatory interleukin 6 cytokine production. Furthermore, we investigated the role of the protein corona on controlling the internalization efficiency in immune cells — we found that the adsorption of serum proteins, in particular haptoglobin, alpha-1-antitrypsin and apolipoprotein A-II, onto the non-PEGylated glycoplexes, significantly reduced the uptake of the glycoplexes by PBMCs. Moreover, the non-PEGylated glycoplexes were efficient in the nuclear factor kappa-light-chain-enhancer of activated B cells (NF-κB) knockdown in monocytic THP-1 cell line. This study provides an insight into the rational design of glycogen-based nanocarriers for the safe delivery of siRNA without eliciting unwanted immune cell activation and efficient siRNA activity upon its delivery.

Keywords: glycogen nanoparticles, siRNA glycoplexes, peripheral blood mononuclear cells, THP-1, phagocytosis, protein corona, stochastic optical reconstruction microscopy

1. Introduction

Achieving controlled and effective delivery of RNA therapeutics, i.e., small-interfering RNA (siRNA), microRNA, messenger RNA (mRNA), and CRISPR/Cas9 mRNA, to different organs for the prevention and treatment of various diseases remains a major translational challenge.[1,2] The direct systemic injection of naked RNA therapeutics is hampered by RNA nuclease degradation in the extracellular environment, fast renal clearance, poor cellular uptake, and unintended side and off-target effects.[2] Hence, the translation of RNA therapeutics in clinical settings requires the development of safe and effective nanocarriers. A wide range of nanocarriers for the encapsulation of RNA molecules have been engineered in the last decades using cationic polymers (e.g., polyethyleneimine (PEI) and dendrimers),[3] cell-penetrating peptides, and inorganic- (e.g., calcium phosphate and silica),[4,5] and lipid-based nanoparticles (NPs).[6] However, there are biological barriers that limit the efficient and safe delivery of RNA cargo to the cytosolic molecular machinery *in vivo*. These include the sequestration of the RNA-loaded nanocarrier by the reticuloendothelial system (i.e., mononuclear phagocytes and Kupffer cells), the limited ability of nanocarriers to cross the capillary endothelium at the desired organ/tissue by transcytosis, unspecific cellular uptake, and inefficient endosomal escape of the nanocarrier and RNA payload.[7] In addition, uncontrolled immune activation induced by the nanocarrier building block is undesirable for RNA therapeutic applications such as protein replacement therapies and genome editing.[8]

Lipid NPs (LNPs) have been extensively investigated and recently applied in clinical settings in mRNA-based vaccines and for the delivery of siRNA therapeutics. [6] However, the synthetic lipid components and moieties in LNPs may activate host immune responses following systemic or local administration that could induce hypersensitivity reactions by stimulating the complement system and secretion of pro-inflammatory cytokines.[9,10] For example, the first United States Food and Drug Administration-approved LNP–siRNA drug, Onpattro, requires premedication with steroids and antihistamines to abrogate unwanted immune reactions.[11]

It has been established that the physicochemical properties of NPs are key to determining their interactions with plasma proteins and immune cells, and the resulting immune response and organ biodistribution.[12] Therefore, understanding the interaction of NPs with immune cells can provide opportunities to rationally design RNA-based nanocarriers with reduced immune activation and controlled biodistribution.

We recently explored the use of a carbohydrate-based NP, namely glycogen, as a promising platform for the alteration of gene expression and transcription.[13–16] Glycogen is a randomly hyperbranched high-molecular weight polysaccharide composed of chains of α-D-(1−4) glucose units that are interlinked by α-D-(1–6) glycosidic linkage to form a dendrimer-like NP.[16] These biological NPs, 20–80 nm in diameter, are obtained commercially through extraction processes from animal tissues or sweet corn on a large scale. Glycogen NPs have several advantageous properties, such as biocompatibility, biodegradability, high water solubility, and hydroxyl functional groups, that make them well suited for use as nucleic acid delivery systems.[17–20] We have demonstrated the preparation and application of cationic glycogen NPs (from bovine liver glycogen, BG) modified with ethylenediamine (EDA) and polyethylene glycol (PEG) moieties (BG-EDA and BG-EDA-PEG NPs) to deliver siRNA and downregulate target gene expression (by ~60%) in prostate tumor spheroids.[13] In addition, by using a single-molecule localization super-resolution microscopy technique, we have shown that glycogen–siRNA constructs (referred to as glycoplexes) undergo endosomal escape *via* the proton-sponge effect in prostate cancer cells.[14] Following intravenous injection in mice, the engineered glycoplexes did not induce toxicity, and exhibited an *in vivo* circulation lifetime of 8 h and preferential accumulation in the liver with negligible sequestration by the spleen.[13]

In the present study, we sought to investigate the interactions of glycoplexes with immune cells. Specifically, we analyzed the interactions of glycoplexes with four major human peripheral blood mononuclear cells (PBMCs) subsets, i.e., monocytes, T cells, B cells, and natural killer (NK) cells, and the intracellular trafficking of the glycoplexes in monocytes. We unveiled the role of the protein corona in controlling the phagocytosis of the glycoplexes by immune cells and siRNA transfection efficiency. This study provides an insight into the rational design of nucleic acid delivery platforms based on glycogen as a promising biological and versatile NP devoid of inflammatory immune response and cytotoxic effects.

2. Materials and methods

Buffy coats were obtained from the Department of Transfusion & Tissue Medicine of the Brno University Hospital (Brno, Czech Republic). Bovine liver glycogen, EDA, sodium cyanoborohydride, sodium metaperiodate, sodium azide, filipin from *Streptomyces filipinensis* (*S. filipinensis*), 5-(N-ethyl-N-isopropyl)-amiloride (EIPA), cytochalasin D from *Zygosporium masonii*, Dulbecco's phosphate buffered saline (PBS), human serum from human male AB plasma, radioimmunoprecipitation assay (RIPA) buffer, goat anti-rabbit peroxidase antibody,

(4′,6-diamidine-2′-phenylindole dihydrochloride), Triton X-100, Tween 20 and bovine serum albumin (BSA) were purchased from Sigma-Aldrich (MO, USA). Pitstop 2 was purchased from Abcam (MA, USA). Dialysis tubing (10 kDa molecular weight cutoff) and protease inhibitor cocktail were purchased from Thermo Fisher Scientific (Victoria, Australia). Alexa Fluor NHS dyes (488, 555, and 647), Lipofectamine 2000, Live/Dead Fixable Near IR stain, trypsin, and rabbit anti-NF-κB p105/p50 polyclonal antibody were purchased from Life Technologies (Victoria, Australia). Methoxypolyethylene glycol amine was obtained from JenKem Technology (TX, USA). RPMI-1640 and X-Vivo 15 media were purchased from Lonza (Allendale, NJ, USA). Fetal bovine serum (FBS) was purchased from Bovogen Biologicals Pty. Ltd. (Victoria, Australia). Illustra NAP-10 columns were purchased from GE Healthcare and Life Sciences (New South Wales, Australia). Polyvinylidene fluoride (PVDF) membrane was obtained from Pall Corporation (Victoria, Australia). Wortmannin, zymosan, and lipopolysaccharide (LPS-EB – LPS from *Escherichia coli* O111:B4) were purchased from InvivoGen (CA, USA). Anti-CD3, anti-CD14, anti-CD57, anti-CD19, and anti-CD20 antibodies were purchased from eBioscience (Thermo Fisher Scientific, MA, USA). Paraformaldehyde (PFA) solution (4%) was obtained from ProSciTech (Queensland, Australia). The NF-κB siRNA (siNF-κB) (sense, 5′-GGG UAU AGC UUC CCA CAC U[dTdT]-3′; antisense, 5′-AGU GUG GGA AGC UAU ACC C[dTdT]-3′) was purchased from Sigma-Aldrich (MO, USA). The control scrambled siRNA (scrRNA) (sense, 5′-GCA CCA UCU UCU UCA AGG A[dTdT]-3′; antisense, 5′-UCC UUG AAG AAG AUG GUG C[dTdT]-3′) was purchased from Thermo Fisher Scientific (Victoria, Australia). Clarity ECL substrate was obtained from Bio-Rad Laboratories (CA, USA). Rabbit anti-β-actin and rabbit anti-LAMP1 monoclonal antibodies were purchased from Cell Signalling Technology (MA, USA). All chemicals were used as received without further purification. High-purity water with a resistivity of >18.2 MΩ cm was obtained from a three-stage Millipore Milli-Q plus 185 purification system (Millipore Corporation, MA, USA). THP-1 human peripheral blood monocytes (TIB-202) were obtained from the American Type Culture Collection. THP-1 cells were regularly tested against mycoplasma contamination and were used below 10 passages.

2.1. Minimum information reporting in bio–nano experimental literature (MIRIBEL)

The studies conducted herein, including material characterization, biological characterization, and experimental details, conform to the MIRIBEL reporting standard for bio–nano research.[21] We include a companion checklist of these components in the Supporting Information.

2.2. Synthesis of BG-EDA and BG-EDA-PEG NPs

BG-EDA and BG-EDA-PEG NPs were synthesized as previously described.[13] Briefly, 100 mg BG was dispersed in 5 mL of 0.6 M acetate buffer (pH 5.0) to which sodium metaperiodate (26 mg, 0.12 mmol) was subsequently added. The reaction was continued for 2 h in the dark. Then, 36 mg (0.6 mmol) EDA or 70 mg (0.035 mmol) methoxy-PEG-amine (2 kDa) was added, followed by the addition of 76 mg sodium cyanoborohydride (1.2 mmol). The reaction was conducted for 16 h, and products were purified by dialysis against Milli-Q water for 3 days and freeze-dried. The degree of substitution of modified glycogen was determined by NMR. BG-EDA: ^{1}H-NMR (400 MHz, D_2O, 78 °C) δ (ppm): 5.316 (s, 0.8H, $H_{1–4}$), 5.11 (s, 0.05H, $H_{1–4'}$), 4.99 (s, 0.1H, $H_{1–6'}$), 4.91 (s, 0.04H, $H_{1–6}$), 4.16–3.44 (m, 11H, H_2, H_3, $H_{4'}$, H_5), 3.38 (t, J = 8 Hz, 0.1H, H_4), 3.26–2.41 (m, 1.65H, H_A, H_B). BG-EDA-PEG: ^{1}H-NMR (400 MHz, D_2O, 78 °C) δ (ppm): 5.35 (s, 0.8H, $H_{1–4}$), 5.16 (s, 0.1H, $H_{1–4'}$), 5.03 (s, 0.03H, $H_{1–6'}$), 4.95 (s, 0.08H, $H_{1–6}$), 4.10–3.50 (m, 6.4H, H_2, H_3, $H_{4'}$, H_5), 3.41 (t, J =8 Hz, 0.12H, H_4), 3.21–2.77 (m, 0.5H, H_A, H_B), 2.21 (s, 6.5H, H_c), 1.89 (s, 0.07H, H_d).

2.3. Labelling of BG-EDA and BG-EDA-PEG NPs with Alexa Fluor NHS dyes

BG-EDA or BG-EDA-PEG (10 mg) NPs were dissolved in 2 mL of 0.1 M sodium bicarbonate buffer (pH 8) and mixed with 100 µL of 1 mg mL^{-1} Alexa Fluor 488 NHS dye with stirring for 2 h in the dark. Excess dye was removed by purification on a NAP-10 filter column and freeze-dried. Dual-labelled glycoplexes were obtained as follows: BG-EDA or BG-EDA-PEG (2 mg) NPs were dissolved in 0.5 mL of 0.1 M sodium bicarbonate buffer (pH 8) and mixed with 20 µL of 1 mg mL^{-1} Alexa Fluor 488 NHS dye and 10 µL of 1 mg mL^{-1} Alexa Fluor 647 NHS dye with stirring for 2 h in the dark. Excess dye was removed on NAP-5 filter columns. For further analysis, the fluorescence intensity of the BG-EDA-PEG NPs was normalized to the fluorescence intensity of the BG-EDA NPs.

2.4. Preparation and characterization of glycoplexes

The formation of BG-EDA-siRNA and BG-EDA-PEG-siRNA glycoplexes was assessed by 10% tris-borate-EDTA polyacrylamide gel electrophoresis (TBE-PAGE). Briefly, siRNA was diluted in 30 mM PBS to a concentration of 1 µM, and 15 pmol NF-κB p105/p50 silencer siRNA was mixed with BG-EDA or BG-EDA-PEG NPs at different weight ratios (2–7) in 30 mL 30 mM PBS buffer. The prepared samples were equilibrated for 10 min on the bench, and 5 mL nucleic acid loading buffer was added. Then, 25 µL of each sample was separated by

TBE-PAGE for 1 h at 150 V and evaluated by SYBR Gold reagent staining and visualization with a ChemiDoc XRS+ Imaging System (BioRad, USA). The ζ-potential of the resulting glycoplexes was measured using a Zetasizer Nano-ZS (Malvern Instruments, Malvern, UK). Finally, 750 mL of a particle dispersion (3 mg mL^{-1}) in Milli-Q water was introduced into a folded capillary cell (DTS1070, Malvern Instruments) and measurements were performed using standard operating procedures with automatic attenuation and measurement position.

For the characterization of the glycoplexes, BG-EDA–siRNA and BG-EDA-PEG-siRNA glycoplexes were prepared using AF647-conjugated glycogen. Then, 400 μL of the glycoplexes (5 μg mL^{-1}) was transferred to Labtek 8-well chamber slides coated with PEI. Stochastic optimal reconstruction microscopy (STORM) images were acquired using a Nikon N-STORM system configured to achieve total internal reflection fluorescence (TIRF) imaging. The focus and TIRF angle were adjusted and tuned to maximize the signal-to-noise ratio. Fluorophores were excited by 488, 561, and 647 nm laser lines. Fluorescence was collected through a Nikon 100× 1.4 NA oil immersion objective. For each channel, 5000 frames were acquired and analyzed using the STORM module of the NIS Elements Nikon software.

2.5. Isolation and analysis of interaction of PBMCs with glycoplexes

PBMCs from four healthy donors were isolated from fresh buffy coats (Department of Transfusion & Tissue Medicine of the University Hospital Brno, Brno, Czech Republic) by density gradient centrifugation in Lymphoprep medium, according to the manufacturer's recommendation.

Isolated PBMCs were plated in 24-well plates with a seeding density of 1×10^6 cells per well in 1 mL X-Vivo 15 media and equilibrated for 30 min at 37 °C. Then, PBMCs were treated with 5 μg mL^{-1} Alexa Fluor 488-labelled glycoplexes, corresponding to 10 pmol of siRNA, at different time points. Cells were then transferred to a V-bottom 96-well plate, centrifuged (350 *g*, 5 min), and washed twice with flow cytometry staining buffer (FACS) buffer (1% FBS in PBS). Cells were stained on ice for 30 min using titrated concentrations of CD19, CD20 (biotin, streptavidin BV421), CD14 (PE), CD57 (PE-Cy7), and CD 3 (APC-Cy7) antibodies. Cells were washed twice with cold PBS, acquired using flow cytometry (BD FACSCanto II) and data were analyzed using FlowJo v.10 (BD Biosciences).

2.6. Mechanism of internalization of glycoplexes by FACS

Isolated PBMCs were seeded in 24-well plates (1×10^6 cells per well) in 1 mL X-Vivo 15 medium and pre-incubated with cytochalasin D (10 µM), wortmannin (100 nM), sodium azide (120 mM), filipin from *S. filipinensis* (5 µg mL^{-1}), pitstop 2 (12 µg mL^{-1}), and EIPA (15 µg mL^{-1}) for 30 min. Then, Alexa Fluor 488-labelled glycoplexes (5.4 µg mL^{-1} final concentration) were added and incubated for 1 h. PBMCs were stained as described above and analyzed by flow cytometry (BD FACSCanto II) and data were analyzed using FlowJo v.10.

2.7. Isolation of monocytes and confocal microscopy imaging

After isolation of PBMCs as previously stated, monocytes were obtained using a Pan Monocyte Isolation Kit, human (Miltenyi Biotec, Germany) according to manufacturer's instruction. The isolated monocytes were resuspended at a density of 4×10^6 cells mL^{-1} in X-Vivo 15 media enriched with inactivated human serum in different concentrations where indicated. Aliquots (30 µL) of the solutions were pipetted into Ibidi channel slides (6-well µ-Slide VI 0.5). Cells were then incubated for 2 h with Alexa Fluor 488-labelled BG-EDA-siRNA or BG-EDA-PEG-siRNA glycoplexes. Monocytes were fixed for 15 min using 4% PFA. After three washes with PBS, cell membranes were stained for 10 min with 5 µg mL^{-1} of wheat germ agglutinin, Alexa Fluor 633 conjugate (Thermo Fisher Scientific, MA, USA) diluted in PBS.

2.8. Effect of protein corona on internalization of glycoplexes by PBMCs

Isolated PBMCs were plated in 24-well plates at a seeding density of 1×10^6 cells per well in 1 mL X-Vivo 15 media with increasing proportion of human serum (2%, 5%, 10%, 20%, and 50%) and equilibrated for 30 min at 37 °C. Then, PBMCs were treated with 5 µg mL^{-1} Alexa Fluor 488-labelled BG-EDA-siRNA or BG-EDA-PEG-siRNA glycoplexes for 2 h at 37 °C. Cells were then transferred to a V-bottom 96-well plate, centrifuged (350 *g*, 5 min), and washed twice with FACS buffer (1% FBS in PBS). Cells were stained on ice for 30 min using titrated concentrations of CD19, CD20 (biotin, streptavidin BV421), CD14 (PE), CD57 (PE-Cy7), and CD 3 (APC-Cy7) antibodies. Cells were washed twice with cold PBS, acquired using flow cytometry (BD FACSCanto II) and data were analyzed using FlowJo v.10.

2.9. Intracellular trafficking analysis of BG-EDA–siRNA and BG-EDA-PEG–siRNA glycoplexes by STORM

Human monocytic THP-1 cells were seeded in 24-well plates (1×10^5 cells per well) in RPMI-1640 medium and left for 30 min for recovery. Dual-labelled (Alexa Fluor 488/Alexa Fluor 647) BG-EDA–siRNA and BG-EDA-PEG–siRNA glycoplexes were added to the cells (5.4 µg

241 mL^{-1} final concentration) and incubated for 2 h. Then, the non-internalized glycoplexes were
242 removed by centrifugation (500 *g*, 5 min, 4 °C) and cells were incubated in a complete medium
243 for an additional 2 h. For analysis, cells were washed twice with PBS, fixed with 4% PFA for
244 20 min, and then washed twice again with PBS, with centrifugation (1000 *g*, 10 min, 4 °C)
245 performed after each step. Cells were resuspended in 400 µL PBS and transferred to poly-L-
246 lysine-coated LabTek 8-well chamber slides and left for 1.5 h to adhere to the glass surface.
247 Then, the cells were permeabilized with 0.1% Triton X-100 in PBS for 5 min, washed trice
248 with PBS, and incubated with a rabbit anti-LAMP1 monoclonal antibody (2.5 µg mL^{-1}) for 1.5
249 h at room temperature. Unbound antibody was washed out thrice with PBS and incubated with
250 a secondary dual-labelled (Alexa Fluor 555/Alexa Fluor 647) goat anti-rabbit monoclonal
251 antibody. After 1 h, the cells were washed thrice with PBS. STORM images were acquired
252 using a Nikon N-STORM system configured to achieve TIRF imaging as described above.

253 **2.10. Interleukin 6 (IL-6) enzyme-linked immunosorbent assay (ELISA)**

254 PBMCs were plated in a 96-well plate (1×10^5 cells per well) in 100 µL X-Vivo 15 media.
255 Monocytes were isolated using a Pan Monocyte Isolation Kit, according to the manufacturer's
256 protocol. BG-EDA-siRNA or BG-EDA-PEG-siRNA glycoplexes were added to a final
257 concentration of 5.4 µg mL^{-1}. Zymosan and lipopolysaccharide (LPS) were added at a final
258 concentration of 1 µg mL^{-1}, and Lipofectamine 2000 was added at the amount equivalent to
259 loaded 10 pmol of siRNA, as described as per the manufacturer's instructions. Cells were
260 incubated with all reagents for 6 h and then the culture supernatant was collected. A commercial
261 DuoSet ELISA (R&D Systems) was used to detect IL-6 in the supernatants. ELISA was
262 performed as per the manufacturer's instructions.

263 **2.11. Cell viability**

264 Isolated PBMCs were prepared as previously described for FACS analysis and incubated with
265 the BG-EDA-siRNA or BG-EDA-PEG-siRNA glycoplexes (5 µg mL^{-1}) for 24 h. Cells were
266 treated with anti-CD14 antibody (PE) and Live/Dead Fixable Near IR stain according to the
267 manufacturer's instructions. The viability of the monocyte population was assessed by flow
268 cytometry (BD FACSCanto II) and the data were analyzed using FlowJo v.10.

269 **2.12. NF-κB p105/p50 Knockdown**

270 THP-1 cells were plated in 12-well plates (8.0×10^4 cells per well). Transfection with BG-
271 EDA–siRNA or BG-EDA-PEG–siRNA glycoplexes was performed with an equivalent of 100

nM siRNA specific to NF-κB p105/p50 (siNF-κB) or a scrambled control siRNA (scrRNA) in Opti-MEM. The efficiency of NF-κB p105/p50 knockdown was evaluated by flow cytometry, 72 h post-transfection. After that time, the cells were washed with PBS by centrifugation (500 *g*, 5 min), fixed with 4% PFA, permeabilized using 0.1% Triton X-100 and 1% BSA in PBS, and stained with a rabbit anti-NF-κB p105/p50 polyclonal antibody (1:200) for 2 h. Goat anti-rabbit Alexa Fluor 488-conjugated antibody (1:200) was used for secondary staining. The cells were washed twice with 1% BSA in DPBS and centrifuged (1000 *g*, 10 min) between each step. The cells were analyzed using a BD Accuri C6 flow cytometer, registering 10000 events per sample. The data were analyzed using FlowJo v.10.

2.13. Western blotting

Western blotting was performed as previously described.[22] Briefly, THP-1 cells were transfected with BG-EDA-siRNA or BG-EDA-PEG-siRNA glycoplexes at a concentration equivalent to 100 nM siRNA and incubated for 72 h. The whole-cell extract was prepared using RIPA buffer containing protease inhibitor cocktail. Proteins were separated by sodium dodecyl sulfate–polyacrylamide gel electrophoresis (SDS-PAGE) and transferred to a PVDF membrane using standard protocols. NF-κB p105/p50 and β-actin were visualized with anti-NF-κB p105/p50 (1:2000 in 1% BSA/1X Phosphate-Buffered Saline, 0.1% Tween® 20 Detergent, PBS-T) and anti-β-actin primary antibodies (1:5000 in 1% BSA/PBS-T). The membrane was then incubated with anti-rabbit peroxidase-conjugated antibody (1:10000 in PBS-T). Bound antibodies were detected using Clarity Western ECL substrate and imaged with a ChemiDoc XRS+ imaging system.

2.14. Protein corona adsorption and analysis

BG-EDA–siRNA or BG-EDA-PEG–siRNA glycoplexes were mixed with human serum (30%) at a final concentration of 25 μg mL^{-1} of glycogen and incubated at 37 °C for 30 min. To separate constructs from free proteins, 300 μL of the mixture was loaded on a size-exclusion chromatography column (height = 16 cm) filled with Sepharose 4b resin (Sigma) equilibrated with PBS and 25 fractions of 250 μL were collected. Human serum (30%) was used as a control. Protein concentration in each fraction was assessed using Pierce BCA Protein Assay Kit (Life Technologies, Australia) as per manufacturer's protocol. After this, 20 μL of combined fractions 8–12, identified as glycoplex–protein corona complexes, were analyzed by SDS-PAGE using 4–20% gradient polyacrylamide gel at 150 V for 40 min. The resulting gels

were stained with SimplyBlue SafeStain (Life Technologies, Australia) and imaged with a ChemiDoc XRS + Imaging System.

2.15. Mass spectrometry and protein identification

Samples for mass spectrometry analysis were prepared following a previously published digestion protocol.[23] Liquid chromatography with tandem mass spectrometry (LC-MS/MS) was carried out on a Q Exactive Plus Orbitrap mass spectrometer (Thermo Scientific) with a nano-electrospray ionization interface in conjunction with an Ultimate 3000 RSLC nano HPLC (Dionex Ultimate 3000). The LC system was equipped with an Acclaim Pepmap nano-trap column (Dinoex-C18, 100 Å, 75 µm × 2 cm) and an Acclaim Pepmap RSLC analytical column (Dinoex-C18, 100 Å, 75 µm × 50 cm). The tryptic peptides were injected into the enrichment column at an isocratic flow of 5 µL min^{-1} of 2% v/v CH_3CN containing 0.1% v/v formic acid for 5 min applied before the enrichment column was switched in line with the analytical column. The eluents were 0.1% v/v formic acid (solvent A) and 100% v/v CH_3CN in 0.1% v/v formic acid (solvent B). The flow gradient was (i) 0–6 min at 3% B, (ii) 6–40 min at 3–25% B, (iii) 40–48 min at 25–45% B, (iv) 48–50 min at 40–80% B, (v) 50–53 min at 85–85% B, (vi) 53–54 min at 85–3% B and equilibrated at 3% B for 10 min before the next sample injection. The Q Exactive Plus mass spectrometer was operated in the data-dependent mode, whereby full MS1 spectra were acquired in positive mode, 70000 resolution, automatic gain control (AGC) target of $3e^6$ and maximum injection time (IT) of 50 ms. Fifteen of the most intense peptide ions with charge states ≥2 and an intensity threshold of $1.7e^4$ were isolated for MS/MS. The isolation window was set at 1.2 *m*/*z* and precursors fragmented using normalized collision energy of 30, 17500 resolution, AGC target of $1e^5$, and maximum IT of 100 ms. Dynamic exclusion was set to be 30 s. Data analysis was carried out using the MaxQuant platform [24] and the Andromeda search engine (version 1.5.3.30), and searched against the UniProt human database (October 2018). The default settings for a label-free quantification (LFQ) experiment with "LFQ", "Match between runs" and intensity-based absolute quantification (iBAQ) features enabled. The false discovery rate was set to 1% on peptide spectrum match and protein level. A minimum of two peptides per protein were required for quantitation. Three replicates of each sample were analyzed, and only proteins that were identified in at least two replicates were evaluated for abundance. The protein contents (mol% of total proteins) for semiquantitative assessment of protein abundance were calculated using equation 1.

$$mol\%_A = \frac{iBAQ_A}{iBAQ_{sum}} \quad (1)$$

where mol%$_A$ is the content of protein A, iBAQ$_A$ is the intensity-based absolute quantification value of protein A, and iBAQ$_{sum}$ is the sum of iBAQ values of all the identified proteins.[23,25–27]

3. Results and discussion

3.1. Glycoplexes predominantly associate with peripheral blood monocytes *ex vivo*

Glycoplexes were prepared as previously described using 20 nm BG NPs.[13] Briefly, BG NPs were modified with EDA and PEG (2 kDa) to obtain positively charged BG-EDA and BG-EDA-PEG NPs by periodate oxidation and subsequent reductive amination reactions. The degree of substitution with EDA (40%) and PEG (2.5%) was evaluated by ^{1}H NMR analysis. Next, two types of siRNA glycoplexes were prepared by electrostatic complexation of BG-EDA and BG-EDA-PEG NPs with a scrambled siRNA sequence (**Figure 1A**).

The glycoplexes were ~137 nm (BG-EDA–siRNA) and ~145 nm (BG-EDA-PEG-siRNA) in size, as determined using STORM, and exhibited a slightly negative surface charge (−4 mV) (**Figure 1A and 1B**). The stability and integrity of both glycoplexes against hydrolytic enzymes and serum proteins were previously investigated:[13,14] both glycoplexes are stable in serum, do not aggregate, disassemble or degrade, and maintain a size of 140 ± 30 nm (BG-EDA-siRNA) or 190 ± 40 nm (BG-EDA-PEG-siRNA).[13] Nevertheless, the adsorption of serum proteins onto glycoplexes and their role in controlling their interactions with immune cells has remained elusive.

To investigate the interactions of the engineered glycoplexes with immune cells, PBMCs were isolated from buffy coats obtained from four healthy blood donors and incubation of the immune cells with the Alexa Fluor 488-labelled glycoplexes (5 µg mL^{-1}) was performed as shown in **Figure 1C**. The cells were stained with specific surface markers for the detection of four major immune cell subsets (monocytes, T cells, B cells, and NK cells) by flow cytometry (**Figure 1D**). A significant association of both glycoplexes with monocytes was observed (>55 % of positive cells). In contrast, moderate interactions with B cells (~36 % of positive cells) and limited interactions (<17 % of positive cells) with T cells and NK cells were observed after a 2 h incubation period (**Figure 1E**). Although the cell association is observed, especially with B cells, the fluorescence intensities for glycoplexes associated with monocytes are ten

magnitudes higher than for other analyzed cell subsets, indicating that the detected fluorescence signal arises from the glycoplexes non-specifically bound to the cell surface.

To gain insight into the association kinetics, the interactions between the glycoplexes and PBMCs were studied as a function of incubation time (**Figure 1F**). A progressive increase in the level of association of both glycoplexes with PBMCs was observed up to 24 h of incubation, confirming the prominent association of glycoplexes with monocytes. Interestingly, the PEGylated glycoplexes showed a higher and faster association with monocytes compared to the non-PEGylated glycoplexes, suggesting that PEGylation facilitates phagocytosis in monocytes. This finding is in stark contrast to numerous studies that have shown that the surface modification of NPs with PEG chains decreases non-specific serum protein adsorption onto the surface of NPs, resulting in a reduced phagocytic uptake by macrophages and monocytes and prolonged circulation time of PEGylated NPs.[28] Our finding suggests that the adsorption of serum proteins onto the surface of glycoplexes may play a pivotal role in mediating the interactions of glycoplexes with monocytes, thus prompting the subsequent investigation on the characterization of the cellular uptake mechanism of glycoplexes and composition of the protein corona.

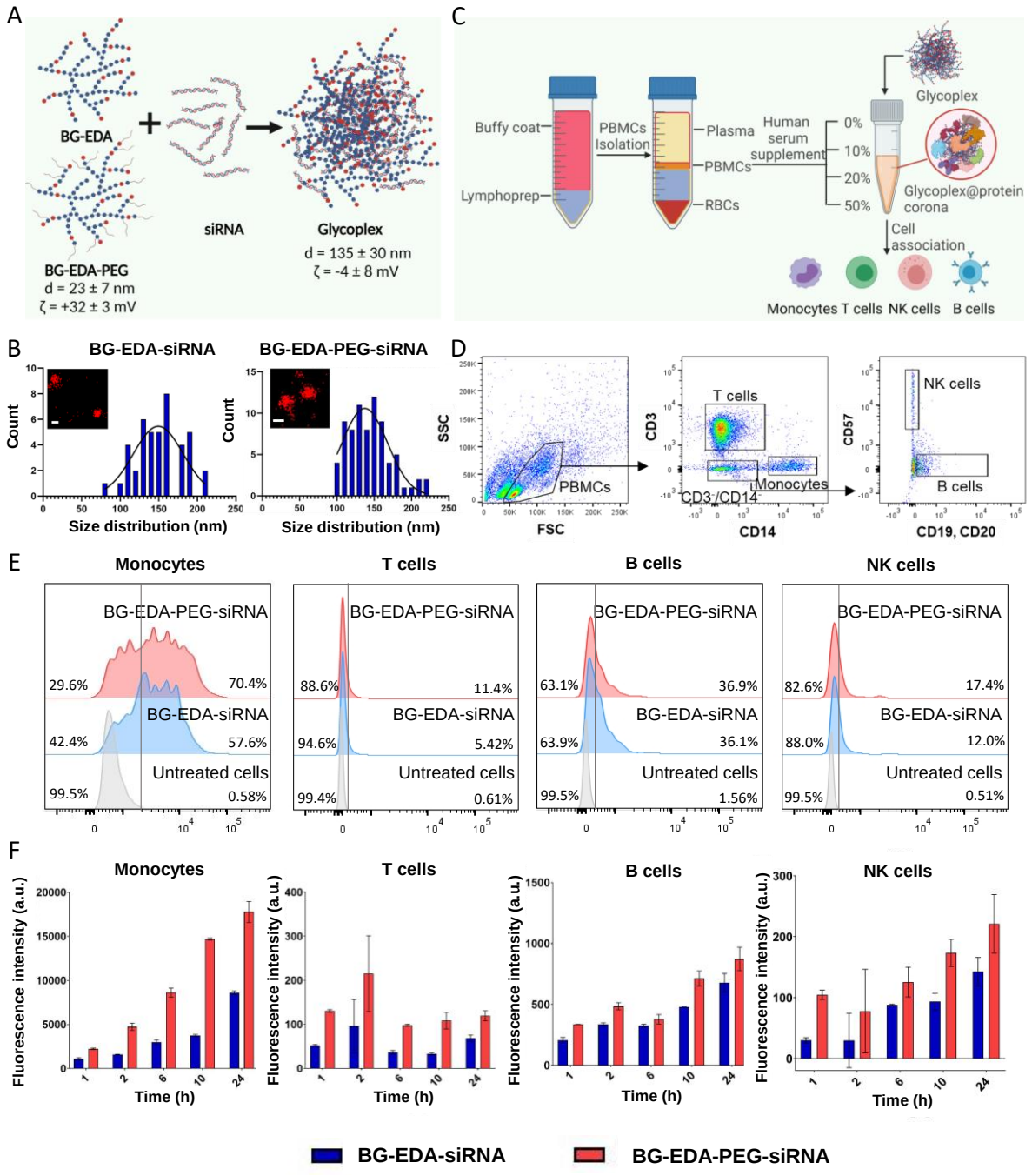

Figure 1. Glycoplexes: characterization and interaction with immune cells. (**A**) Schematic of formation of glycoplexes. (**B**) Size distributions (n = 80) of BG-EDA–siRNA and BG-EDA-PEG-siRNA glycoplexes at siRNA-to-glycogen (w/w) ratios of 4 and 6, respectively, analyzed by STORM. (**C**) Schematic of isolation of PBMCs from buffy coats and experimental layout for studying protein corona-dependent cell association with human blood-isolated immune cells. RBCs, red blood cells. (**D**) Representative flow cytometry gating strategy used for monocytes, T cells, B cells, and NK cells. (**E**) Histograms showing the association of the glycoplexes (FITC channel) and percentage of positive cell population after incubation for 2 h

with different PBMCs subsets: $CD14^+$ monocytes, $CD3^+$ T cells, $CD19^+CD20^+$ B cells, and $CD57^+$ NK cells. (**F**) Cell association kinetic plots of BG-EDA–siRNA and BG-EDA-PEG-siRNA glycoplexes with $CD14^+$ monocytes, $CD3^+$ T cells, $CD19^+CD20^+$ B cells, and $CD57^+$ NK cells. Autofluorescence from untreated cells was subtracted from the plots and is reported as 623, 98, 114, and 123 a.u. for monocytes, T cells, B cells, and NK cells, respectively. Fluorescence of BG-EDA and BG-EDA-PEG NPs was normalized. Data represent the means ± standard deviations (SDs). A and C were created with BioRender.com.

3.2. Glycoplexes are internalized in monocytes by phagocytosis

To elucidate the specific endocytic pathway used by the glycogen–siRNA glycoplexes to enter monocytes, we studied the effects of inhibiting phagocytosis and micropinocytosis, using the inhibitors wortmannin and cytochalasin D respectively, on NP internalization (**Figure 2A and 2B**).

Cytochalasin D disrupts actin microfilaments and blocks actin polymerization during phagocytosis and macropinocytosis),[22] whereas wortmannin inhibits phosphatidylinositol 3-kinase (PI3K) and subsequent signalling pathways leading to membrane and cytoskeleton reorganization during micropinocytosis.[29] PBMCs isolated from three donors were pre-incubated with either cytochalasin D or wortmannin for 45 min. Both glycoplexes were then incubated with PBMCs for 1 h and cell association was assessed by flow cytometry. Regardless of the inhibitor treatment or type of glycoplex used, no significant inhibition in internalization was observed in T cells, B cells, and NK cells (**Figure 2A**). These data, together with the minor association observed before, suggest that the glycoplexes are not actively internalized by these subsets of immune cells but rather bind to the cell membranes. The limited uptake by the difficult-to-transfect immune cells was also observed for other NP systems.[30]

Unlike the other immune cells tested, a reduced uptake of the BG-EDA–siRNA and BG-EDA-PEG-siRNA glycoplexes was observed by monocytes pretreated with cytochalasin D but no inhibitory effects were observed in response to wortmannin (**Figure 2A**). This decrease in internalization (by 90%) after cytochalasin D treatment suggests that phagocytosis might be the exclusive mechanism responsible for the internalization of the constructs.

To unequivocally rule out the possible involvement of endocytosis in capturing glycoplexes by monocytes, we extended our studies to inhibitors specific to endocytic pathways. Pitstop 2 and filipin from *S. filipinensis* were used to inhibit clathrin- and caveolae-dependent endocytosis,

respectively, and EIPA was used to inhibit macropinocytosis. In addition, PBMCs were incubated with sodium azide to block all energy-dependent internalization pathways (**Figure 2B**). Incubation with sodium azide inhibited internalization completely, confirming that the glycoplexes are taken up by either endocytosis or phagocytosis in monocytes rather than by passive diffusion or membrane fusion pathways. The results also showed that clathrin- and caveolae-dependent endocytosis pathways were not involved in the internalization of the glycoplexes, whereas EIPA inhibited BG-EDA–siRNA glycoplex uptake by ~30%, suggesting a partial involvement of micropinocytosis. Nonetheless, the internalization of BG-EDA-PEG-siRNA glycoplex was not inhibited by EIPA, indicating that phagocytosis is the predominant pathway employed by monocytes for the uptake of PEGylated glycoplexes in blood.

As monocytes and other myeloid cells are specialized in ingesting foreign materials by active phagocytosis,[31] the involvement of the phagocytotic pathway in the internalization of the glycoplexes by monocytes is expected. However, the internalization pathways of glycoplexes in immune cells differ from those identified in epithelial cells. For example, we have previously shown that PC3 prostate cancer cells primarily uptake BG-EDA–siRNA and BG-EDA-PEG-siRNA glycoplexes *via* caveolae-mediated endocytosis and macropinocytosis.[14]

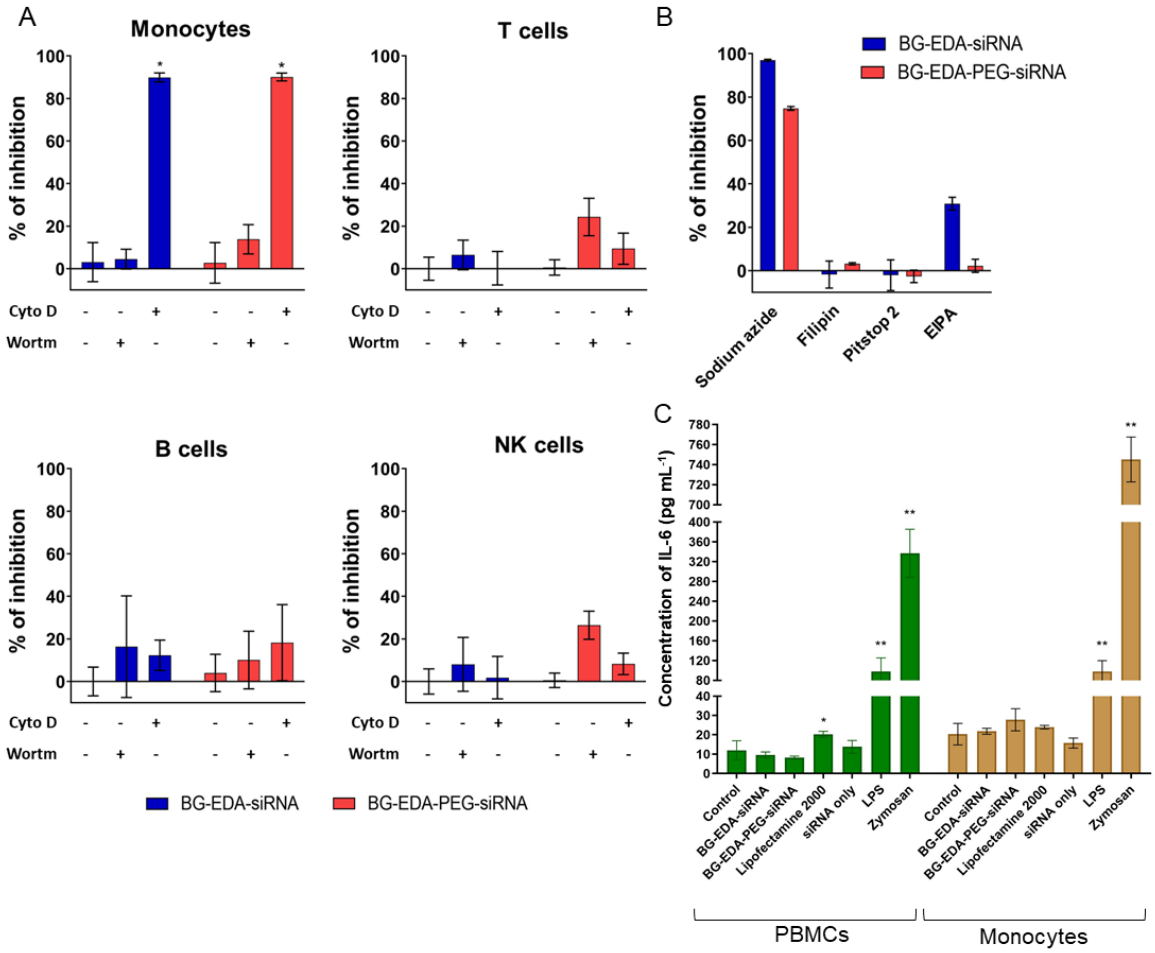

437

438 **Figure 2. Glycoplexes are phagocytosed by monocytes without triggering the**
439 **inflammatory signalling cascade event.** (**A**) Effect of inhibitors of phagocytosis on glycoplex
440 internalization by PMBCs. PBMCs were incubated with cytochalasin D (Cyto D) or
441 wortmannin (Wortm), and internalization by monocytes, T cells, B cells, and NK cells was
442 monitored by flow cytometry. The data are expressed as percentage of induced inhibition
443 (±SD). Statistical significance was determined by a two-tailed *t*-test against untreated control
444 cells. **p* < 0.05, *n* = 3. (**B**) Effect of inhibitors of internalization processes on the uptake of
445 glycoplexes by monocytes. The data are expressed as percentage of induced inhibition (±SD).
446 (**C**) IL-6 expression levels in whole PBMCs and isolated monocytes after stimulation with
447 glycogen–siRNA glycoplexes, Lipofectamine 2000, LPS, or zymosan. IL-6 levels were
448 determined by ELISA after 6 h of incubation. The data represent the means ± SDs. Statistical
449 significance was determined by two-way analysis of variance (ANOVA) against untreated cell
450 control. **p* < 0.05 and ***p* < 0.01, *n* = 3.

3.3. Glycoplexes enter immune cells without triggering the inflammatory signalling cascade event

The cytotoxicity of the glycoplexes and their ability to activate an immune response were examined. The effect of the type and concentration of the glycoplexes on monocyte survival was first monitored by flow cytometry after stimulating the whole PBMC population for 24 h (**Figure S1**). The BG-EDA–siRNA glycoplex did not display any cytotoxic effects on monocytes within the range of glycogen concentrations examined. However, a gradual decrease in monocyte viability was observed after treatment with the BG-EDA-PEG-siRNA glycoplex to 80% at the highest concentration (100 μg mL^{-1}) examined.

The recognition of foreign materials by phagocytes can lead to cell activation, cytokine production, and immune response. Here, we used IL-6 as a marker of inflammation: it is primarily produced by monocytes and is regulated downstream of NF-κB, which is activated upon cell stimulation by most pathogens. By ELISA, we monitored IL-6 levels after 6 h incubation of the glycoplexes using scrRNA with whole PBMCs or isolated monocytes (**Figure 2C**). Both glycoplexes were compared with the siRNA transfection reagent, Lipofectamine 2000. Toll-like receptor (TLR) ligands, such as LPS and zymosan, were used as positive controls to activate IL-6 expression in myeloid cells. Upon incubation of both glycoplexes with whole PBMCs or monocytes, we did not observe any significant increase in IL-6 levels. In contrast, a small but statistically significant increase in IL-6 levels was noticed after treating whole PBMCs with lipofectamine (from 10 pg mL^{-1} for untreated PBMCs to 20 pg mL^{-1} after treatment with lipofectamine), but monocyte activation by lipofectamine was not observed. As expected, LPS and zymosan significantly increased IL-6 levels in the culture media, confirming the capacity of the tested cells to produce IL-6 upon NF-κB activation.

These results suggest that glycoplexes interact with immune cells without triggering the inflammatory signalling cascade event. The maintenance of a steady-state status in myeloid cells provides a potentially important advantage to glycoplexes over other systems, such as lipid-based materials that can perturb myeloid cell signalling, causing cell activation and changes in the transcriptional program.[32,33] The absence of activated cell signalling or a stress response upon interaction of the glycoplexes with immune cells possibly arises from the ubiquitous presence of this endogenous polysaccharide in the body as a cellular energy storage molecule. In summary, glycoplexes seem to be a promising system to deliver siRNA *in vivo* without triggering unwanted immunogenic responses and side effects.

3.4. Human serum proteins modulate the interactions of glycoplexes with PBMCs

To investigate the effect of human serum proteins on the uptake of glycoplexes by PBMCs, we evaluated the level of internalization of both glycoplexes into PBMCs in the presence of an increasing concentration of human serum from 0 to 50 % (**Figure 3A and Figure S2**). As observed from **Figure 3A**, both the association of BG-EDA–siRNA glycoplex with monocytes and the proportion of monocytes positive for BG-EDA–siRNA glycoplex decreased with an increasing amount of human serum. In contrast, no significant change in the association efficiency and the proportion of positive monocytes was observed for the BG-EDA-PEG-siRNA glycoplex (**Figure 3A**) when quantified by flow cytometry. The effective internalization of both glycoplexes into monocytes was further confirmed by confocal microscopy (**Figure 3B**) and by 3D reconstruction (**Figure S3**) as shown in the representative images. Taken together, these results indicate that the interaction between primary monocytes and the BG-EDA–siRNA glycoplex is minimized in the presence of serum proteins. Conversely, BG-EDA-PEG-siRNA association with monocytes is unaffected by the presence of serum proteins. Although association was limited, a decreasing trend was observed when either of the glycoplexes was incubated with the other immune cell subsets (T cells, B cells, and NK cells) in human serum at increasing concentrations (**Figure S2**). The results appear to suggest that PEGylation steadies the phagocytosis in monocytes in the presence of human serum. This effect has been reported in human neutrophils in the presence of human serum *in vitro*.[28]

To obtain an insight into the role of serum proteins in the internalization efficiency of the glycoplexes, a mass spectrometry proteomics study and SDS-PAGE were performed to analyze the content of the protein corona (**Figure 3C and 3D**). The glycoplexes were first incubated with human serum and isolated from the excess of proteins by size-exclusion chromatography (SEC) (**Figure S4**). Analysis of the protein content in each collected fraction showed that the glycoplex–protein corona complexes exited the SEC column in the void volume, in fractions 8–12, whereas human serum proteins remained within the resin and eluted in fraction 13 and onward. Therefore, fractions 8–12 for each eluted sample were combined, and SDS-PAGE was performed. The SDS-PAGE image in **Figure 3D** indicates the absence of proteins in the combined fractions when human serum was eluted from the SEC column. Conversely, a high abundance of proteins was observed on the gel for BG-EDA–siRNA and BG-EDA-PEG-siRNA glycoplexes, suggesting that glycoplex–protein corona complexes are successfully isolated from unbound serum proteins. It is widely reported that PEG grafting typically leads

to a decrease in total protein adsorption on NPs although it cannot completely prevent protein corona formation.[34] As expected, PEGylation of the glycoplexes reduced the adsorption of all serum proteins (**Figure 3D** and **Figure S4**). However, mass spectrometry analysis of adsorbed proteins expressed as percentage of total protein revealed a similar protein corona composition in the PEGylated and non-PEGylated glycoplexes (**Figure 3C**). Analysis of the protein corona stripped from the glycoplexes revealed the presence of serum albumin, haptoglobin, alpha-1-antitrypsin, and immunoglobulins as the main components of the protein corona. There was a limited amount of complement proteins (<1 mol%) enriched in the protein coronas of glycoplexes with or without PEGylation. Albumin is the most abundant negatively charged protein in serum and its adsorption onto glycoplexes is likely driven by electrostatic interactions or hydrogen bonding between the hyperbranched polysaccharide chains and the protein domains. An increase in the relative molar abundance of albumin and lower amounts of haptoglobin and alpha-1-antitrypsin were observed on the PEGylated glycoplexes. Although albumin is regarded as a dysopsonin, it has been shown that the dysopsonin properties can be overruled by strong opsonins such as immunoglobulins.[35] Interestingly, haptoglobin and alpha-1 antitrypsin might play a role in reducing the phagocytosis of the non-PEGylated glycoplexes. Generally, haptoglobin has been reported to have an anti-inflammatory effect on monocytes expressing CD163 (heme/haptoglobin scavenger receptor), which enables endocytosis of heme/haptoglobin complexes,[36,37] and alpha-1-antitrypsin has been reported to be a key protein to facilitate efficient clearance of apoptotic neutrophils by macrophages.[38] Furthermore, we observed more immunoglobulins (Ig kappa chain C region and Ig gamma-1 chain C region) and less apolipoprotein A-II enriched in the corona of the PEGylated glycoplexes than that of the non-PEGylated counterparts, which could be attributed to their higher monocyte association in the presence of human serum. This is consistent with our previous finding and current literature on the key proteins associated with immune recognition.[23,30] Immunoglobulins known as opsonins were found to opsonize foreign materials and promote phagocytosis,[39,40] whereas apolipoproteins regarded as dysopsonins may compete for surface binding with opsonins to reduce phagocytosis.[41,42] This is also supported by recent studies that show that apolipoprotein corona on NPs have dysopsonizing activity, which prevents phagocytosis or act as a protective shell to minimize the degradation of transfected oligonucleotides.[34,43]

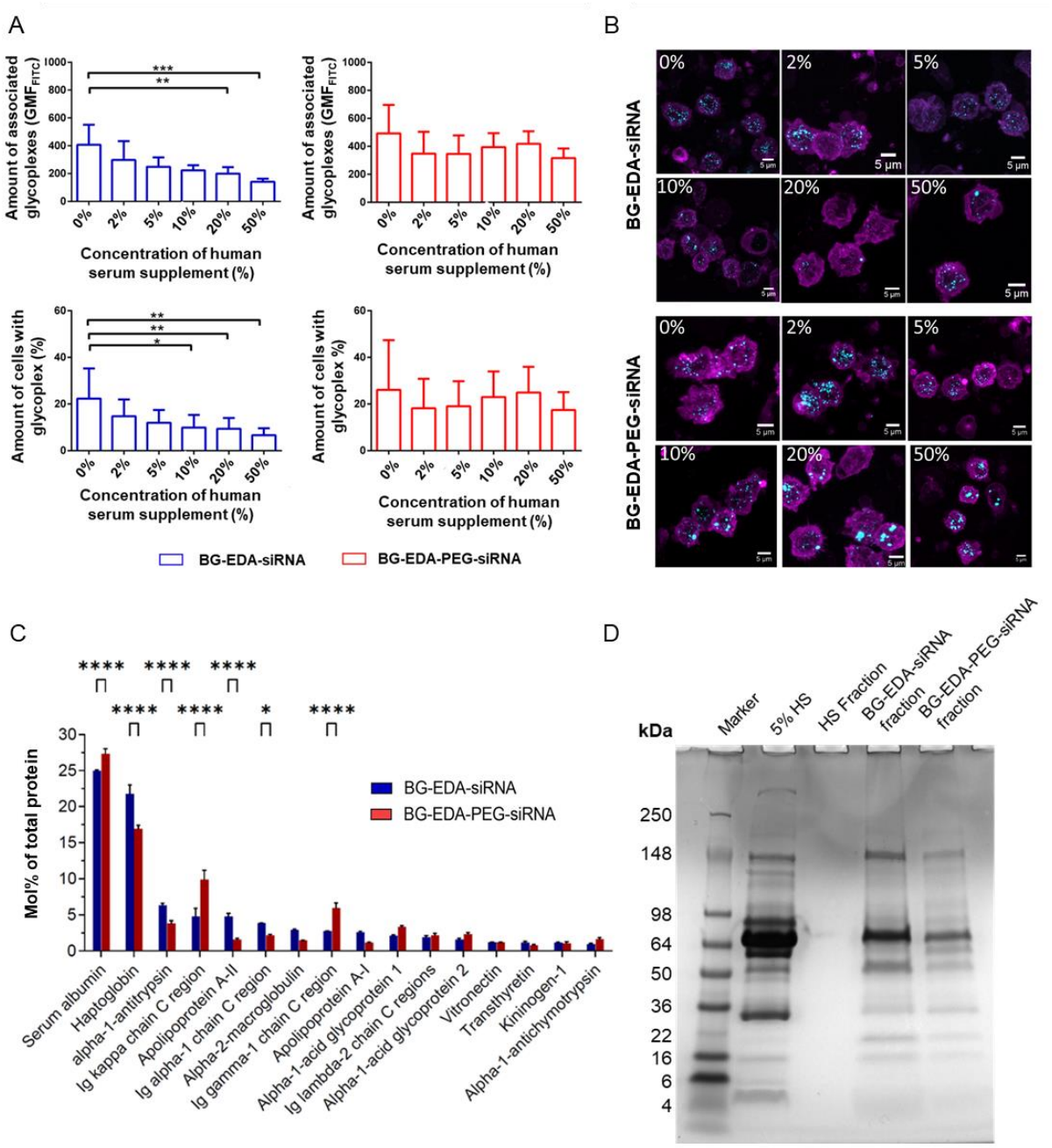

Figure 3. Serum protein adsorption reduces the interaction of siRNA glycoplexes with monocytes. (**A**) Internalization of BG-EDA–siRNA and BG-EDA-PEG-siRNA glycoplexes by human monocytes treated with human serum. Bar charts represent the amount of internalized FITC-labelled particles (top) and the percentage of $FITC^+$-cells (bottom). The data represent the means ± SDs (n = 5). Statistical significance was determined by Friedman test with Dunn's multiple comparison test against 0% of human serum supplement cell control. *p < 0.05, **p < 0.01, and ***p < 0.001. (**B**) Maximum intensity projections showing internalization of BG-EDA-siRNA and BG-EDA-PEG-siRNA glycoplexes by monocytes treated with different concentration of human serum. Glycoplexes are depicted in cyan and cell

membrane in magenta. (**C**) LC-MS/MS analysis of protein corona composition of BG-EDA and BG-EDA-PEG glycoplexes after incubation with human serum. Protein contents (mol% of total proteins) were calculated from the iBAQ values. The most abundant proteins (>1 mol%) are shown in the figure. Data are shown as the means ± SDs (n = 3). *p < 0.05, ****p < 0.0001 (two-way ANOVA with Tukey's multiple comparisons test). (**D**) SDS-PAGE image of combined fractions 8–12 collected from SEC columns. Human serum (5% HS) was used as a control.

3.5. Glycoplexes are capable of lysosomal escape and NF-κB knockdown in THP-1 monocytic cell line

The intracellular trafficking of glycoplexes upon phagocytosis by THP-1 monocytes was investigated using STORM, following transfection for 2 or 4 h (**Figure 4A and 4B**). Phagocytosis typically involves the processing of ingested particles through lysosomal compartments before subsequent degradation.[44] BG-EDA–siRNA and BG-EDA-PEG-siRNA glycoplexes were labelled with an Alexa Fluor 488/Alexa Fluor 647 activator–reporter pair, and the lysosomes were labelled with an anti-LAMP1 and Alexa Fluor 555/Alexa Fluor 647 tandem dye system. This enables the simultaneous imaging and tracking of the glycoplexes and lysosomes.

In the analyzed cells, we imaged different nano-objects (**Figure 4C**) for each time point including (i) glycoplexes not localized with lysosomes, (ii) glycoplexes co-localized with lysosomes, (iii) glycoplexes in the proximity of lysosomes suggesting lysosome rupture, and (iv) non-colocalized/empty lysosomes. At both 2 and 4 h time points, glycoplexes co-localized and non-colocalized with LAMP1-positive compartments (lysosomes) were observed and quantified (**Figure S5)**. Although we cannot discriminate between glycoplexes localized within LAMP1-negative compartments (e.g., phagosomes) and those in the cytosol, these results suggest that endosomal escape of both glycoplexes likely occurs after incubation for 2 h. We have shown that the osmotic swelling and subsequent mechanical stress of early endosomal vesicles of PC3 cells cause the formation of large pores that facilitate the release of glycoplexes in the cytosol.[14] Furthermore, BG-EDA is endowed with pH-sensitive amine (pK$_a$ of ~6.4) functionalities that cause the proton-sponge effect by buffering the inner core of early and late endosomes during endocytosis.[13,14] During the phagocytosis of glycoplexes into THP-1 cells, the transition from the phagosomes to the lysosomes is accompanied by a decrease in pH from ~7.5 to ~4.9.[44] The STORM images of glycoplexes non-colocalized with lysosomes within

589 THP-1 cells suggest that the translocation of glycoplexes from the lysosome to the cytosol
590 might be facilitated by the proton-sponge effect mechanism.

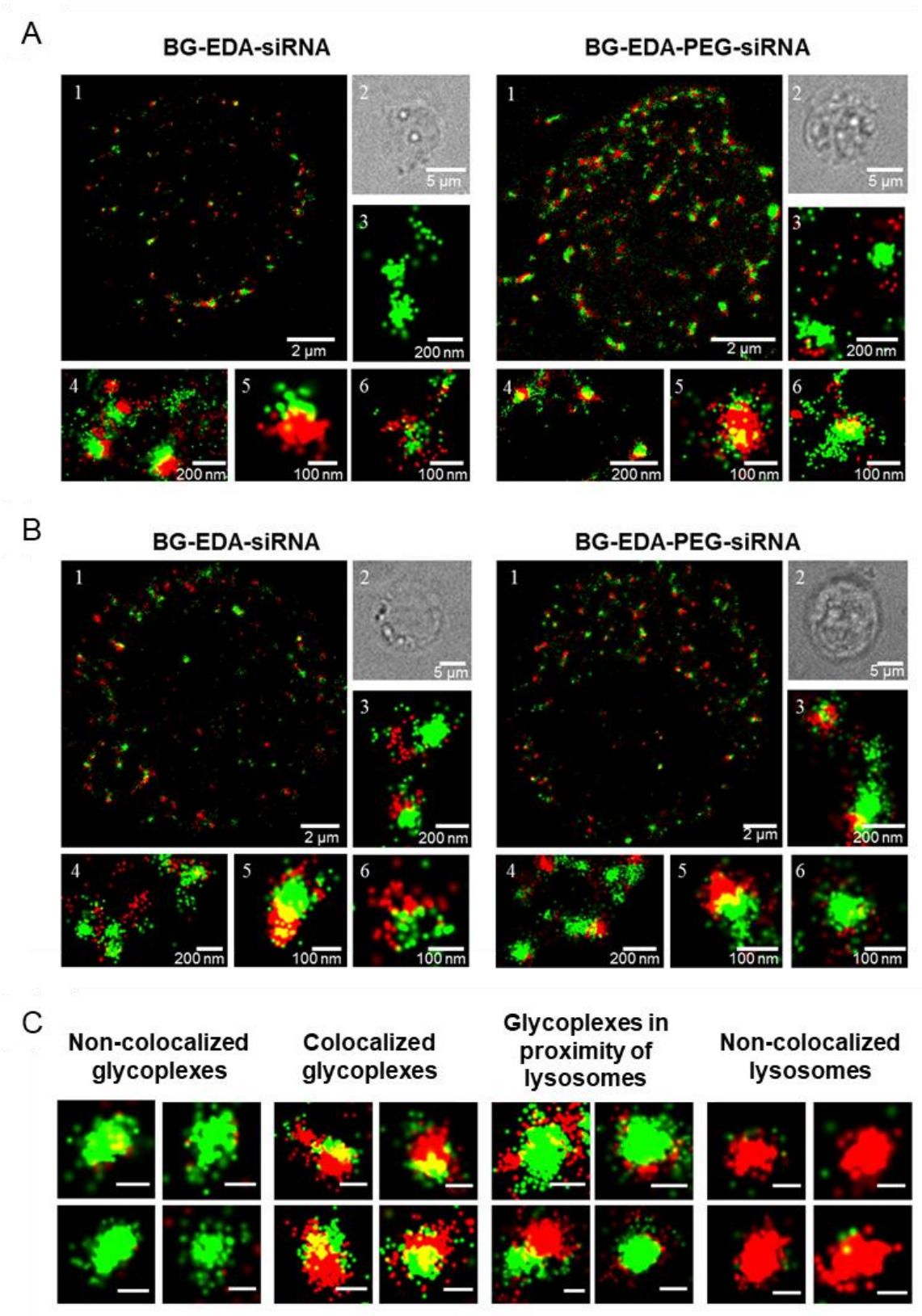

591

Figure 4. Glycoplexes are capable of lysosomal escape in THP-1 monocytic cell line. Representative multicolour STORM images of glycogen–siRNA glycoplexes and LAMP-1-positive lysosomes, at each time point, n=8 cells and n=100 nano objects/cell were analyzed. (**A, B**) THP-1 monocytes were incubated with BG-EDA–siRNA or BG-EDA-PEG-siRNA glycoplexes for 2 h (**A**) or 4 h (**B**). Image 1, large view of a representative THP-1 cell; image 2, bright-field image of the presented THP-1 cell; images 3–6, high-magnification images showing details of intracellular nano-objects. (**C**) Classification of nano-objects identified by STORM image analysis. Four distribution patterns showing non-co-localized glycoplexes, glycoplexes co-localized with lysosomes, glycoplexes in the proximity of ruptured lysosomes, and non-colocalized/empty lysosomes after incubation for 2 h with glycoplexes. Scale bars are 100 nm. BG-EDA–siRNA and BG-EDA-PEG-siRNA glycoplexes are labelled with Alexa Fluor 488/Alexa Fluor 647 (green), and lysosomes are labelled with anti-LAMP1 dual-labelled Alexa Fluor 555/Alexa Fluor 647 (red).

Following lysosomal escape, the BG-EDA–siRNA and BG-EDA-PEG-siRNA glycoplexes are expected to deliver bioactive cargo to the cell. To verify this hypothesis, BG-EDA-siRNA and BG-EDA-PEG-siRNA glycoplexes were prepared using siRNA sequence targeting NF-κB p105/p50 protein (siNF-κB) or scrambled sequence (scrRNA) and incubated with THP-1 cells for 72 h. Knockdown was evaluated by flow cytometry by measuring NF-κB immunofluorescence (**Figure 5A and 5B**) and western blotting (**Figure 5C and 5D**). The results showed that the BG-EDA–siNF-κB glycoplex achieved ~40% NF-κB downregulation compared to the BG-EDA-scrRNA. Conversely, no significant downregulation was observed when cells were transfected with the BG-EDA-PEG-siNF-κB glycoplexes compared to the BG-EDA-PEG-scrRNA control. As a positive control, lipofectamine-mediated transfection of siNF-κB was performed and resulted in ~40% NF-κB downregulation (**Figure 5D**). These data confirm that the internalized BG-EDA–siRNA glycoplexes effectively transport siRNA cargo from phagolysosomal compartments to the cytosol and protect the siRNA from nuclease degradation in the lysosomes. The inability of the BG-EDA-PEG-siNF-κB glycoplexes to deliver bioactive siRNA may be attributed to the reduced adsorption of albumin, which protects siRNA from nuclease attack and degradation inside the acidic lysosomal compartments. Overall, these results confirm that the interaction of glycoplexes with serum proteins can play a vital role in minimizing both the non-specific uptake by immune cells and degradation of the nucleic acid cargo in monocytes.

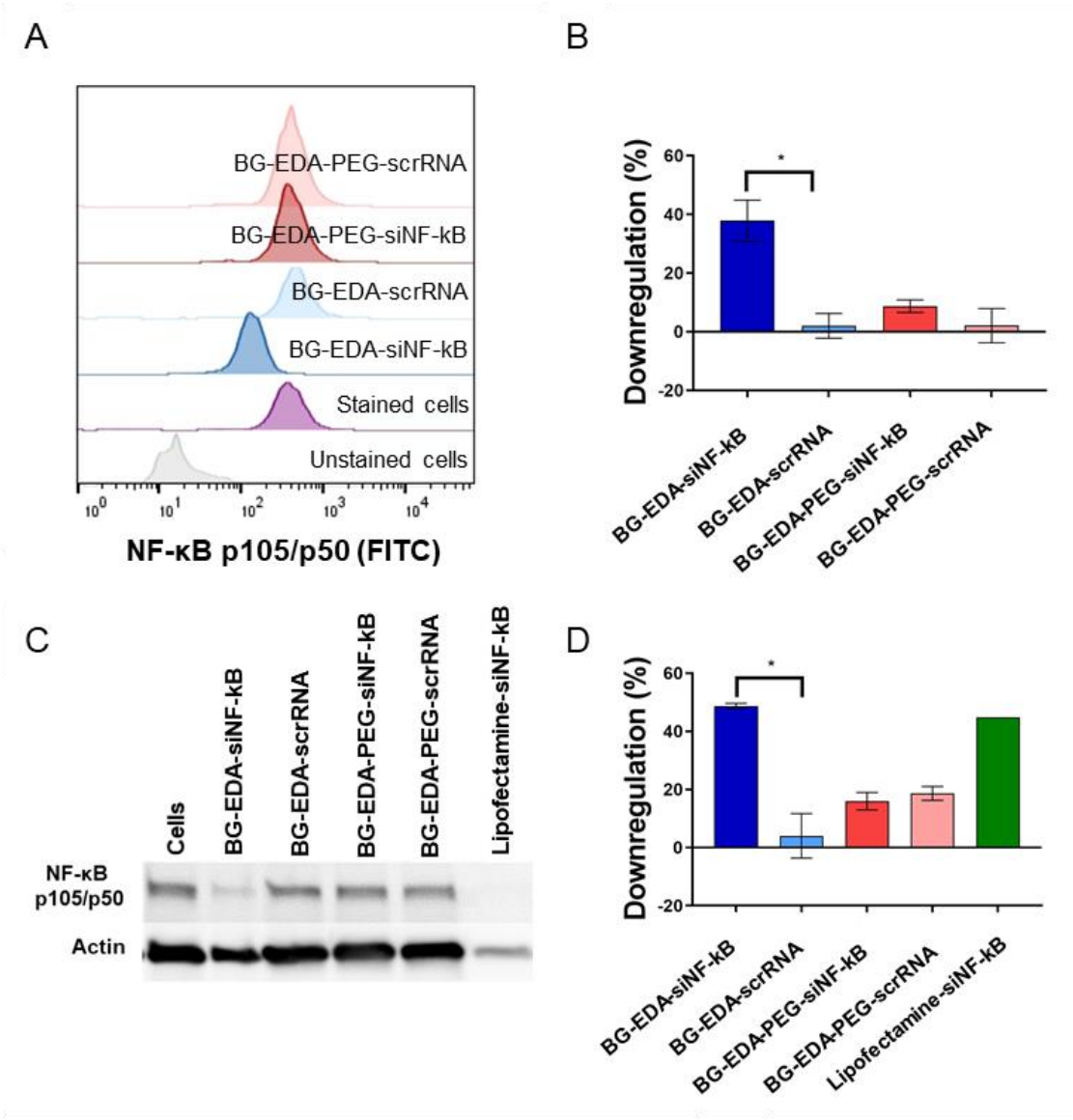

Figure 5. Glycogen NPs effectively deliver siRNA. THP-1 cells were transfected with glycogen–siRNA targeting NF-κB p105/p50 (glycogen-siNF-κB) or scrambled control (glycogen-scrRNA) for 72 h. (**A**) Flow cytometry histograms showing cellular immunofluorescence after staining transfected cells with an anti-NF-κB p105/p50. (**B**) Quantification of NF-κB downregulation by BG-EDA and BG-EDA-PEG measured by flow cytometry. The data represent the means ± SDs. Statistical significance was determined by a two-tailed *t*-test. **p* < 0.05, *n* = 4. (**C**) Representative western blot image of NF-κB p105/p50 protein levels in transfected THP-1 cells. (**D**) Quantification of NF-κB protein levels from western blot images. The data represent the means ± SDs. Statistical significance was determined by a two-tailed *t*-test. **p* < 0.05, *n* = 3.

4. Conclusions

The present study showed that the interaction between glycoplexes and blood-derived PBMCs resulted in the effective internalization of the glycoplexes into primary monocytes by phagocytosis, whereas only limited association with B cells, NK cells, and T cells was observed. The glycoplexes were found to be non-toxic and they did not stimulate endogenous IL-6 cytokine release upon incubation with whole PBMCs or with isolated monocytes. Interestingly, we found that human serum reduced the interaction of the non-PEGylated glycoplexes with monocytes and that the non-PEGylated glycoplexes efficiently silenced NF-κB.

Although proteomics analysis indicated similar protein corona compositions for both the PEGylated and non-PEGylated glycoplexes, the more efficient adsorption of haptoglobin, alpha-1-antitrypsin and/or apolipoprotein A-II onto the non-PEGylated glycoplexes likely contributed to minimizing phagocytosis by monocytes and protecting siRNA from lysosomal degradation. The most NPs are modified to confer stealth properties by attaching PEG chains to create a hydrophilic shield and thus, avoid undesirable immune-system recognition.[45,46] PEG is a non-toxic and non-immunogenic material: PEGylated nanomaterials show an enhanced circulatory half-life, and reduced serum protein absorption (including immunoregulatory proteins) and association with cells compared to non-PEGylated nanomaterials.[45,46] However, many studies have shown that PEGylation shortens the circulation time in the blood, when nanomedicine is repeatedly injected into the same animal host.[47] This accelerated blood clearance phenomenon is explained through the production of anti-PEG antibodies,[47–51] that are in turn possible mediators of enhanced phagocytosis prohibiting the lysosomal escape and NF-κB silencing. Moreover, the anti-PEG antibodies are present in 40-60 % of healthy population,[28] and thus, limiting the use of PEGylated nanomedicines for drug delivery. In conclusion, this study highlights that glycogen is a promising biological nanoparticle that can be easily engineered as a functional platform for the safe delivery of nucleic acids without eliciting immune cell activation and cytotoxic effects.

Conflicts of interest

There are no conflicts to declare.

Acknowledgements

This work was supported by a University of Melbourne Establishment Grant (F. Cavalieri and M.W.). This work was funded by an Australian Research Council (ARC) Future Fellowship (FT140100873, F. Cavalieri), a National Health and Medical Research Council (NHMRC) Senior Principal Research Fellowship (GNT1135806, F. Caruso), and an NHMRC Senior Research Fellowship B (GNT1042059, M.P.). This research was also supported by a European Social Fund and European Regional Development Fund—Project MAGNET (No. CZ.02.1.01/0.0/0.0/15_003/0000492) and project no. LQ1605 from the National Program of Sustainability II (MEYS CR). The Ministry of Health of the Czech Republic - DRO (Institute of Hematology and Blood Transfusion – IHBT, 00023736). This project received funding from the European Union's Horizon 2020 research and innovation programme under the Marie Skłodowska-Curie grant agreement No. 690901. This work was performed in part at the Materials Characterization and Fabrication Platform (MCFP). The authors thank the technical support team at the Center for Translational Medicine (FNUSA-ICRC) for technical support and Insight Editing London for editing the manuscript prior to submission.

Corresponding Authors

*E-mail: fcaruso@unimelb.edu.au.

*E-mail: francesca.cavalieri@unimelb.edu.au.

*E-mail: jan.fric@fnusa.cz.

Supporting information: Viability of monocytes upon association with glycoplexes; association data of T cells, B cells and NK cells with glycoplexes and increasing serum concentration; 3D reconstruction of monocyte association with glycoplexes; elution profile of glycoplex-protein corona; MIRIBEL checklist for reporting research in bio–nano science.

References

[1] T. C. Roberts, R. Langer, M. J. A. Wood, *Nat Rev Drug Discov* **2020**, *19*, 673.

[2] B. Hu, L. Zhong, Y. Weng, L. Peng, Y. Huang, Y. Zhao, X.-J. Liang, *Signal Transduct Target Ther* **2020**, *5*, 101.

[3] V. Dzmitruk, E. Apartsin, A. Ihnatsyeu-Kachan, V. Abashkin, D. Shcharbin, M. Bryszewska, *Pharmaceutics* **2018**, *10*, DOI 10.3390/pharmaceutics10030126.

[4] A. Tabaković, M. Kester, J. H. Adair, *Wiley Interdiscip Rev Nanomed Nanobiotechnol* **2012**, *4*, 96.

[5] H. Meng, W. X. Mai, H. Zhang, M. Xue, T. Xia, S. Lin, X. Wang, Y. Zhao, Z. Ji, J. I. Zink, et al., *ACS Nano* **2013**, *7*, 994.

[6] X. Hou, T. Zaks, R. Langer, Y. Dong, *Nat Rev Mater* **2021**, 1.

[7] H. J. Kim, A. Kim, K. Miyata, K. Kataoka, *Adv Drug Deliv Rev* **2016**, *104*, 61.

[8] M. P. Lokugamage, Z. Gan, C. Zurla, J. Levin, F. Z. Islam, S. Kalathoor, M. Sato, C. D. Sago, P. J. Santangelo, J. E. Dahlman, *Advanced Materials* **2020**, *32*, e1904905.

[9] R. Kedmi, N. Ben-Arie, D. Peer, *Biomaterials* **2010**, *31*, 6867.

[10] A. S. Abu Lila, H. Kiwada, T. Ishida, *J Control Release* **2013**, *172*, 38.

[11] T. Coelho, D. Adams, A. Silva, P. Lozeron, P. N. Hawkins, T. Mant, J. Perez, J. Chiesa, S. Warrington, E. Tranter, et al., *N Engl J Med* **2013**, *369*, 819.

[12] K. A. Dawson, Y. Yan, *Nat Nanotechnol* **2021**, *16*, 229.

[13] M. Wojnilowicz, Q. A. Besford, Y.-L. Wu, X. J. Loh, J. A. Braunger, A. Glab, C. Cortez-Jugo, F. Caruso, F. Cavalieri, *Biomaterials* **2018**, *176*, 34.

[14] M. Wojnilowicz, A. Glab, A. Bertucci, F. Caruso, F. Cavalieri, *ACS Nano* **2019**, *13*, 187.

[15] E. Czuba-Wojnilowicz, S. Miellet, A. Glab, S. Viventi, F. Cavalieri, C. Cortez-Jugo, M. Dottori, F. Caruso, *Biomacromolecules* **2020**, *21*, 3186.

[16] Q. A. Besford, F. Cavalieri, F. Caruso, *Adv Mater* **2020**, *32*, e1904625.

[17] S. A. Engelberth, N. Hempel, M. Bergkvist, *Bioconjug Chem* **2015**, *26*, 1766.

[18] X. Liang, X. Ren, Z. Liu, Y. Liu, J. Wang, J. Wang, L.-M. Zhang, D. Y. Deng, D. Quan, L. Yang, *Int J Nanomedicine* **2014**, *9*, 419.

[19] Z. Liu, H. Gong, R. Zeng, X. Liang, L.-M. Zhang, L. Yang, Y. Lan, *Int J Nanomedicine* **2015**, *10*, 2735.

[20] T. N. Alkie, J. de Jong, K. Jenik, K. M. Klinger, S. J. DeWitte-Orr, *Sci Rep* **2019**, *9*, 13619.

[21] M. Faria, M. Björnmalm, K. J. Thurecht, S. J. Kent, R. G. Parton, M. Kavallaris, A. P. R. Johnston, J. J. Gooding, S. R. Corrie, B. J. Boyd, et al., *Nat Nanotechnol* **2018**, *13*, 777.

[22] C. Lamaze, L. M. Fujimoto, H. L. Yin, S. L. Schmid, *J Biol Chem* **1997**, *272*, 20332.

[23] J. Song, Y. Ju, T. H. Amarasena, Z. Lin, S. Mettu, J. Zhou, M. A. Rahim, C.-S. Ang, C. Cortez-Jugo, S. J. Kent, et al., *ACS Nano* **2021**, *15*, 10025.

[24] S. Tyanova, T. Temu, J. Cox, *Nat Protoc* **2016**, *11*, 2301.

[25] B. Schwanhäusser, D. Busse, N. Li, G. Dittmar, J. Schuchhardt, J. Wolf, W. Chen, M. Selbach, *Nature* **2011**, *473*, 337.

[26] A. B. Saltzman, M. Leng, B. Bhatt, P. Singh, D. W. Chan, L. Dobrolecki, H. Chandrasekaran, J. M. Choi, A. Jain, S. Y. Jung, et al., *Mol Cell Proteomics* **2018**, *17*, 2270.

[27] X. Zeng, J. Sun, S. Li, J. Shi, H. Gao, W. Sun Leong, Y. Wu, M. Li, C. Liu, P. Li, et al., *Nat Commun* **2020**, *11*, 567.

[28] Y. Qie, H. Yuan, C. A. von Roemeling, Y. Chen, X. Liu, K. D. Shih, J. A. Knight, H. W. Tun, R. E. Wharen, W. Jiang, et al., *Sci Rep* **2016**, *6*, 26269.

[29] K. Lindmo, H. Stenmark, *J Cell Sci* **2006**, *119*, 605.

[30] Y. Ju, H. G. Kelly, L. F. Dagley, A. Reynaldi, T. E. Schlub, S. K. Spall, C. A. Bell, J. Cui, A. J. Mitchell, Z. Lin, et al., *ACS Nano* **2020**, *14*, 15723.

[31] N. Oh, J.-H. Park, *Int J Nanomedicine* **2014**, *9 Suppl 1*, 51.

[32] X. Guo, H. Wang, Y. Li, X. Leng, W. Huang, Y. Ma, T. Xu, X. Qi, *Immunol Cell Biol* **2019**, *97*, 92.

[33] A. Fiszer-Kierzkowska, N. Vydra, A. Wysocka-Wycisk, Z. Kronekova, M. Jarząb, K. M. Lisowska, Z. Krawczyk, *BMC Mol Biol* **2011**, *12*, 27.

[34] S. Schöttler, K. Landfester, V. Mailänder, *Angew Chem Int Ed Engl* **2016**, *55*, 8806.

[35] E. Papini, R. Tavano, F. Mancin, *Front Immunol* **2020**, *11*, 567365.

[36] M. S. Arredouani, A. Kasran, J. A. Vanoirbeek, F. G. Berger, H. Baumann, J. L. Ceuppens, *Immunology* **2005**, *114*, 263.

[37] P. Philippidis, J. C. Mason, B. J. Evans, I. Nadra, K. M. Taylor, D. O. Haskard, R. C. Landis, *Circ Res* **2004**, *94*, 119.

[38] J. Lee, Y. Lu, R. Oshins, J. West, C. G. Moneypenny, K. Han, M. L. Brantly, *Front Immunol* **2020**, *11*, 574410.

[39] V. P. Vu, G. B. Gifford, F. Chen, H. Benasutti, G. Wang, E. V Groman, R. Scheinman, L. Saba, S. M. Moghimi, D. Simberg, *Nat Nanotechnol* **2019**, *14*, 260.

[40] H. H. Gustafson, D. Holt-Casper, D. W. Grainger, H. Ghandehari, *Nano Today* **2015**, *10*, 487.

[41] N. Bertrand, P. Grenier, M. Mahmoudi, E. M. Lima, E. A. Appel, F. Dormont, J.-M. Lim, R. Karnik, R. Langer, O. C. Farokhzad, *Nat Commun* **2017**, *8*, 777.

[42] S. Ritz, S. Schöttler, N. Kotman, G. Baier, A. Musyanovych, J. Kuharev, K. Landfester, H. Schild, O. Jahn, S. Tenzer, et al., *Biomacromolecules* **2015**, *16*, 1311.

[43] A. Lacroix, H. H. Fakih, H. F. Sleiman, *J Control Release* **2020**, *324*, 34.

[44] J. Canton, R. Khezri, M. Glogauer, S. Grinstein, *Mol Biol Cell* **2014**, *25*, 3330.

[45] J. M. Harris, R. B. Chess, *Nature Reviews Drug Discovery* **2003**, *2*, 214.

[46] K. Knop, R. Hoogenboom, D. Fischer, U. S. Schubert, *Angewandte Chemie International Edition* **2010**, *49*, 6288.

[47] X. Wang, T. Ishida, H. Kiwada, *Journal of Controlled Release* **2007**, *119*, 236.

[48] T. Ishida, K. Masuda, T. Ichikawa, M. Ichihara, K. Irimura, H. Kiwada, *International Journal of Pharmaceutics* **2003**, *255*, 167.

[49] T. Ishihara, M. Takeda, H. Sakamoto, A. Kimoto, C. Kobayashi, N. Takasaki, K. Yuki, K. Tanaka, M. Takenaga, R. Igarashi, et al., *Pharmaceutical Research* **2009**, *26*, 2270.

[50] E. T. M. Dams, P. Laverman, W. J. G. Oyen, G. Storm, G. L. Scherphof, J. W. M. van der Meer, F. H. M. Corstens, O. C. Boerman, *Journal of Pharmacology and Experimental Therapeutics* **2000**, *292*, 1071.

[51] P. Laverman, M. G. Carstens, O. C. Boerman, E. Th. M. Dams, W. J. G. Oyen, N. van Rooijen, F. H. M. Corstens, G. Storm, *Journal of Pharmacology and Experimental Therapeutics* **2001**, *298*, 607.